

Estimating Spatiotemporal Variation in Ambient Ozone Exposure during 2013–2017 Using a Data-Fusion Model

Tao Xue, Yixuan Zheng, Guannan Geng, Qingyang Xiao, Xia Meng, Meng Wang, Xin Li, Nana Wu, Qiang Zhang,* and Tong Zhu*



Cite This: *Environ. Sci. Technol.* 2020, 54, 14877–14888



Read Online

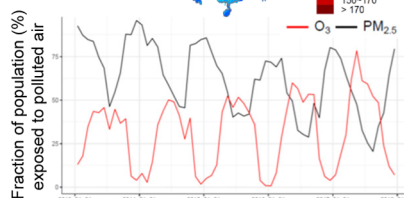
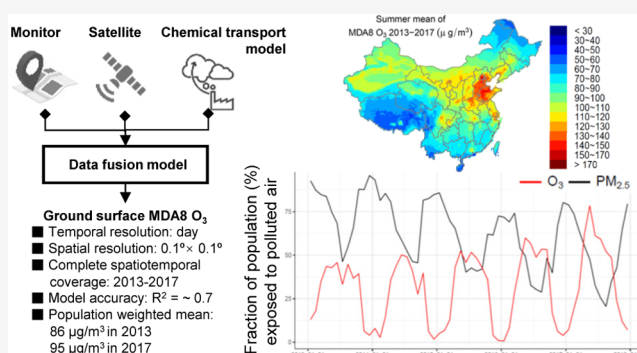
ACCESS |

Metrics & More

Article Recommendations

Supporting Information

ABSTRACT: Since 2013, clean-air actions in China have reduced ambient concentrations of PM_{2.5}. However, recent studies suggest that ground surface O₃ concentrations increased over the same period. To understand the shift in air pollutants and to comprehensively evaluate their impacts on health, a spatiotemporal model for O₃ is required for exposure assessment. This study presents a data-fusion algorithm for O₃ estimation that combines *in situ* observations, satellite remote sensing measurements, and model results from the community multiscale air quality model. Performance of the algorithm for O₃ estimation was evaluated by five-fold cross-validation. The estimates are highly correlated with the *in situ* observations of the maximum daily 8 h averaged O₃ ($R^2 = 0.70$). The mean modeling error (measured using the root-mean-squared error) is 26 $\mu\text{g}/\text{m}^3$, which accounts for 29% of the mean level. We also found that satellite O₃ played a key role to improve model performance, particularly during warm months. The estimates were further used to illustrate spatiotemporal variation in O₃ during 2013–2017 for the whole country. In contrast to the reduced trend of PM_{2.5}, we found that the population-weighted O₃ mean increased from 86 $\mu\text{g}/\text{m}^3$ in 2013 to 95 $\mu\text{g}/\text{m}^3$ in 2017, with a rate of 2.07 (95% CI: 1.65, 2.48) $\mu\text{g}/\text{m}^3$ per year at the national level. This increased trend in O₃ suggests that it is becoming an important contributor to the burden of diseases attributable to air pollutants in China. The developed method and the results generated from this study can be used to support future health-related studies in China.



INTRODUCTION

Exposure to ambient air pollutants, including fine particulate matter (PM_{2.5}) and ozone (O₃), is a key contributor to the global burden of diseases, through harming the human cardiorespiratory system.^{1–3} In China, the central government put a series of emission-control measures into action in 2013 (known as China's clean-air actions)⁴ to mitigate the adverse health impacts of air pollutants and to improve ambient air quality. Such measures include control of coal-fired boiler emissions, promotion of clean fuels in the residential sector, and optimization of the industrial structure, to name a few; these have rapidly reduced PM_{2.5} concentrations on a national scale.^{5,6}

Ground surface O₃ is majorly formed by nonlinear photochemical reactions between volatile organic compounds (VOCs) and nitrogen oxide radicals (NO_x) in the presence of sunlight. Therefore, O₃ is produced rapidly in warm days. Chemical reactions in the atmosphere that drive the formation of O₃ usually depend on the relative levels of VOCs and NO_x and many other factors.^{7,8} Recent studies also suggest that PM_{2.5} can scavenge precursors of O₃ and thus contribute to the growth of O₃.^{7,8} The *in situ* observations have shown that O₃

concentrations were increased during 2013–2017, at a national level.^{7–10} However, due to the sparse distribution of routine pollutant monitors, how trends in O₃ vary between different cities is still unclear. To characterize the nationwide patterns of O₃, an estimation with complete spatiotemporal coverage is necessary.

Epidemiological studies have associated cardiorespiratory diseases with both short- and long-term exposure to ambient O₃.^{11–15} Recent findings have confirmed that the health effects of O₃ exposure are independent of those of PM_{2.5} exposure.¹⁴ Therefore, to comprehensively evaluate the disease burden attributable to air pollutants, the health effects of O₃ exposure should not be ignored. Although there are many studies^{5,6,16} that evaluate risk of exposure to ambient PM_{2.5} in China to understand the health benefits of clean-air actions, assessments

Received: May 14, 2020

Revised: October 26, 2020

Accepted: October 26, 2020

Published: November 11, 2020



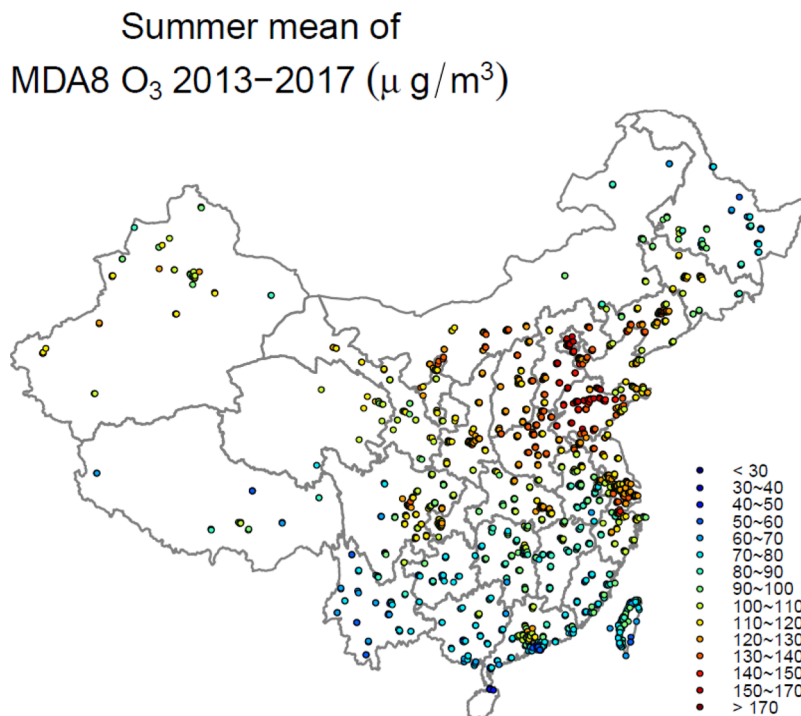


Figure 1. Spatial distribution of *in situ* O₃ monitors in China. Colors indicate MDA8 O₃ averages ($\mu\text{g}/\text{m}^3$) for all summers during 2013–2017.

of the impacts from O₃ exposure are rare. To support such risk assessment studies, a complete spatiotemporal coverage of the corresponding air pollutant is required. For instance, satellite-based maps of annual PM_{2.5} have been applied to quantify long-term exposure and are utilized as an input to exposure-response models,¹⁷ such as the integrated exposure-response model.¹⁸ Previous studies of O₃ are usually based on the output from a chemical transport model (CTM),¹⁹ which might have low accuracy due to the limited data quality of emission inventories.²⁰ In addition, unlike satellite aerosol products, column concentrations of O₃ can be less indicative of ground-surface pollution levels because of the vertical distribution of O₃. Therefore, in contrast to commonly used satellite-based PM_{2.5} products, remote sensing measurements of O₃ have rarely been incorporated into exposure assessment.

Shen *et al.* developed a new indicator for ground-surface O₃ based on satellite measurements, by filtering out the less indicative variables in ozone monitoring instrument (OMI) profiles.²¹ The product is in good agreement with *in situ* observations and covers the most populous areas of China.²¹ Since there are multiple types of numerical O₃ values with different advantages, a statistical approach, which brings them together, can improve accuracy in the O₃ estimates. This study applies a three-stage data-fusion algorithm combining the satellite indicator with many other variables, including *in situ* observations and CTM output. O₃ estimates are first evaluated using cross-validation (CV) and then are used to characterize the spatiotemporal trends of O₃ exposure in China during 2013–2017. Further, we compared the patterns of O₃ to those of PM_{2.5} to explore how the air quality varied after conducting the clean-air actions.

METHODS

Data Inputs. In Situ Observations. We collected multiple monitoring networks of *in situ* hourly observations of O₃ in China, from the China Environmental Monitoring Center

(<http://113.108.142.147:20035/emcpublish/>), the Environmental Protection Department of Hong Kong (<https://cd.epic.epd.gov.hk/EPICDI/air/station/>), and the Taiwan Air Quality Monitoring Network (<https://taqm.epa.gov.tw/taqm/en/default.aspx>). In total, the study includes 1666 unique monitoring sites for the period 2013–2017. For each site, we calculated the maximum daily 8 h average (MDA8) for every day with at least 75% valid hourly O₃ concentrations. This resulted in 2,156,207 values of MDA8 O₃, with a median value of 83.5 $\mu\text{g}/\text{m}^3$ and an interquartile range of 55.8–117.4 $\mu\text{g}/\text{m}^3$, for use in the modeling analyses. The spatial distribution of these monitors is visualized in Figure 1.

CTM Simulations. We simulated continuous spatiotemporal hourly values of O₃ for China during 2013–2017 using the community multiscale air quality (CMAQ) model. Our simulations were applied to derive a fused estimator of PM_{2.5}²² and in other studies of air quality in China.⁵ In the CMAQ model, the anthropogenic emission inventories, which were generated from the multiresolution emission inventory model for China (MEIC), were driven by the climate field output from the weather research and forecasting (WRF) model. Our CMAQ model simulated the chemical species, including O₃, using the CB05 mechanism.²³ CTMs based on MEIC inventories have previously been utilized to explore the spatiotemporal variation in O₃ pollution in China.⁷

The spatial resolution of the WRF-CMAQ model is 36 × 36 km, and hourly simulations of O₃ were calculated as the MDA8 values as an initial input to the data-fusion model. Detailed settings of the WRF-CMAQ model have been documented in our previous publications^{16,22} and are the same for this study. The model also outputs meteorological variables (temperature, relative humidity, height of the planetary boundary layer, wind speed, and pressure) and other ambient pollutants (including nitrogen dioxide [NO₂] and PM_{2.5}). All output variables, apart from O₃, were aggregated into daily mean values. The data-fusion model has a regular grid-spacing of 0.1° × 0.1° covering

all of China. The WRF-CMAQ output was downscaled to this grid spacing using an inverse-distance weighted method,²⁴ where the value at each centroid of the $0.1^\circ \times 0.1^\circ$ grid was calculated as the weighted average of the neighboring pixels in the 36×36 km grid, and the averaging weights were inversely proportional to the corresponding distances.

Satellite Remote-Sensing Measurements. We collected satellite data following the protocol described in a previous study.²¹ First, we obtained the ozone profile (PROFOZ; v0.9.3, level 2) measured by the OMI on the Aura satellite. The PROFOZ contains ozone and other retrieved auxiliary parameters for 24 vertical layers.^{25–27} The Aura is an Earth-observing satellite with a local overpass time of 13:30. The PROFOZ retrieves the O_3 profile with 3–7 vertical layers in the troposphere, and a nadir resolution of 13×24 km, using a Bayesian optimization algorithm.²⁸ The trace of the averaging kernel matrices below a given pressure level [also known as the effective degrees of freedom (DOFs)], which is indicative of the number of independent satellite signals used in the O_3 profile retrieval, can be used to give the accuracy of the corresponding estimates. According to Shen *et al.* (2019),²¹ the O_3 measurements below 400 hPa with DOFs >0.3 are representative of ground-surface MDA8 concentrations across eastern China, the most populous subregion. Given such constraints, the satellite-derived O_3 is in fair correlation ($R = 0.73$) with *in situ* observations during 2013–2017.²¹ After preparing the satellite data as described in the study,²¹ we downscaled the variable onto the $0.1^\circ \times 0.1^\circ$ grid using the inverse-distance weighting approach, same as we used for the WRF-CMAQ output described above.

We also collected other satellite measurements, including the normalized difference vegetation index (NDVI) and night light data. The monthly NDVI data (MOD13A3) were freely obtained from the Application for Extracting and Exploring Analysis Ready Samples (AppEEARS; <https://lpdaacsvc.cr.usgs.gov/apppears/>). The annual night light data in 2013 were measured by visible and infrared sensors as part of the Defense Meteorological Satellite Program and are maintained by the National Centers for Environmental Information (NCEI). To quantify pollutant exposure, we also obtained LandScan population data for 2013 from the Oak Ridge National Laboratory (<https://landscan.ornl.gov/>). The NDVI, night light, and population data had a fine resolution of 1×1 km and were all upscaled to the $0.1^\circ \times 0.1^\circ$ grid for further analyses.

Data Fusion Model. We designed a three-step data fusion model to combine multiple predictors for the daily concentration of ground surface O_3 .

Step 1. First, we developed two separate random forest models.²⁹ One model associates the *in situ* observations with WRF-CMAQ-simulated O_3 and auxiliary variables, including (1) CMAQ outputs of $PM_{2.5}$ and NO_2 , (2) WRF outputs of temperature, relative humidity, wind speed, height of planetary boundary layer, and pressure, (3) satellite measurements of NDVI and night light, and (4) temporal indices. Temporal indices were utilized to characterize the nonlinear temporal trends in O_3 and include the month index and day of the week. Because the model links CMAQ-simulated O_3 to monitoring data, outputs from the random forest model are named CMAQ-calibrated estimates. The second random forest additionally incorporates the satellite-derived O_3 into the first one. The satellite-derived O_3 does not completely fill the spatiotemporal field due to several reasons; for example, the

satellite sensors can be blocked by clouds or affected by issues such as row anomaly. Therefore, the second random forest model generates estimates at the coordinates where the satellite data were available. Given this, the output from the second model is named satellite-based estimates. The random forest approach is capable of modeling complex nonlinear relationships and thus has been utilized to estimate the ground surface O_3 in previous studies. Our random forest models were performed using the R-package *randomForest*.³⁰

Step 2. We combined the two estimators in step 1. As shown in our **Results** section, the satellite-based estimator is more accurate due to the inclusion of an additional predictor, but it does not have 100% coverage. For instance, only 44% of the *in situ* observations could be matched with the valid satellite-derived O_3 measurements. By contrast, the CMAQ-calibrated estimator has a lower accuracy but complete spatiotemporal coverage. To bring the advantages of the two estimators together, we combined them using an elastic-net regression model.³¹ The model regresses the difference between the two estimators for specific dates with a set of two-dimensional spline functions. To avoid overfitting, the regression model is regularized by an elastic-net penalty. By combining the predicted differences and the CMAQ-calibrated estimator, we derived the step 2 estimator (denoted as CMAQ + satellite estimator). The elastic-net model was performed using the R-package *glmnet*.³²

Step 3. We added the stochastic signals of *in situ* observations of O_3 , which are not captured by the above two-stage deterministic estimator, into the final predictions. We assumed that these signals are stable and thus can be characterized by a spatiotemporal correlation function. Therefore, they can be predicted using spatiotemporal Kriging interpolation^{24,33} of the residuals in step 2. A similar geostatistical approach is also known as a small-area estimator.³⁴ Because the deterministic estimators (like those in steps 1 and 2) capture the major spatiotemporal trends in O_3 , they might be less accurate than local measurements when predicting fine-scale variation. The Kriging approach gave the best linear unbiased estimator by combining the deterministic predictions with local measurements. The step 3 estimator is denoted as CMAQ + satellite + monitor.

Cross-Validation. A CV approach has been utilized as the gold standard to evaluate the performance of our model. In this method, a subset of the *in situ* observations was saved for testing data, and the rest was used as the training data to fit the three-stage model. The fitted model was used to generate predictions at the spatiotemporal coordinates of the testing data, and model performance was assessed using various statistics. These included the correlation coefficient [$R^2 = \text{cor}(\text{observation}, \text{prediction})$], mean bias [$\text{bias} = \text{mean}(\text{observation} - \text{prediction})$], root-mean-square error [$\text{RMSE} = \sqrt{\text{mean}(\text{observation} - \text{prediction})^2}$], relative prediction error [$\text{RPE} = \text{RMSE}/\text{mean}(\text{observation})$], and mean absolute error [$\text{MAE} = \text{mean}[\text{abs}(\text{observation} - \text{prediction})]$]. To use all of the data in the comparison, the whole dataset was divided into several subsets, and each of them is used as the testing data one at a time.

We designed different CV tests to examine model performance under different scenarios. First, we utilized five-fold CV (CV_5), which randomly divides all *in situ* observations into five subsets. This approach has been used widely in previous studies, and it represents the scenario where the estimator is used to predict random missing values at some monitoring

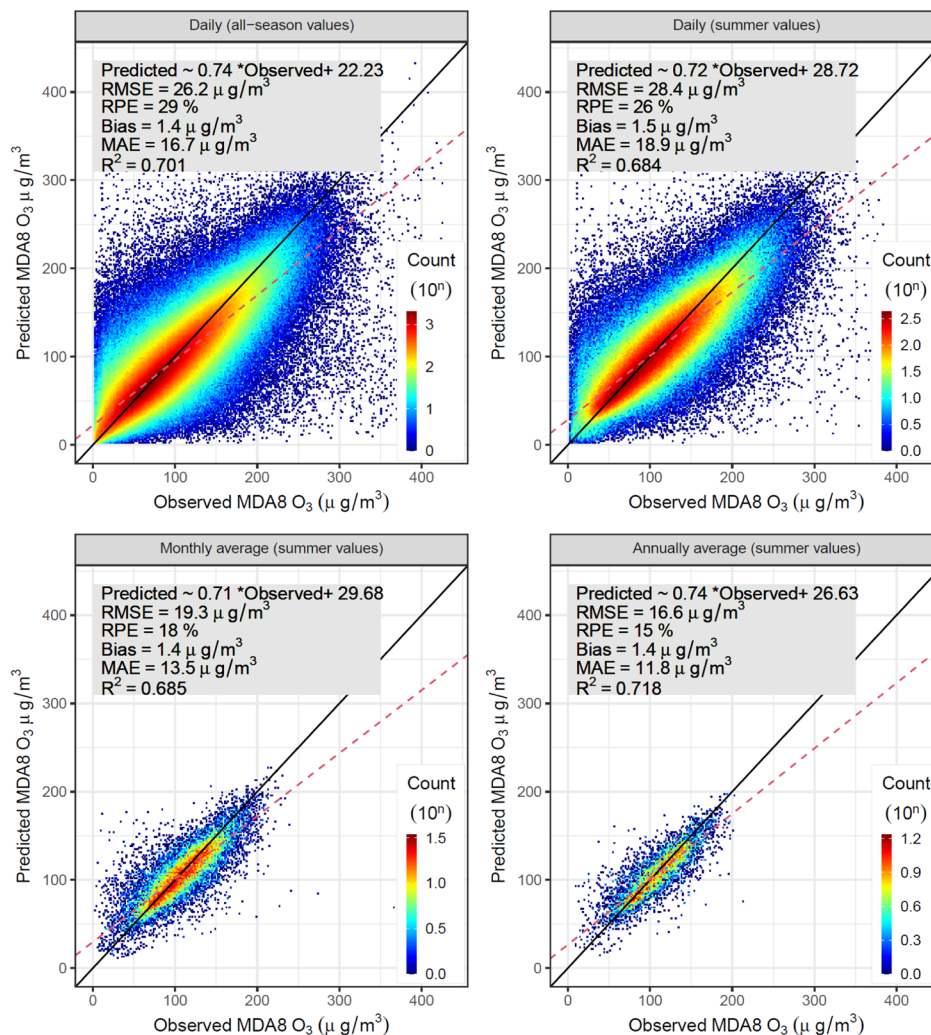


Figure 2. Five-fold CV results for the CMAQ + satellite + monitor estimator of MDA8 O₃ at different time scales.

sites. To mimic the scenario where all monitoring values within a geographic area are not available for a specific date and should be predicted by the model, we designed tests called CV_{county, date} and CV_{city, date}. In such clustered CV tests, *in situ* observations from all monitors within a geographic unit (a county or a city) for a specific date were simultaneously selected as the testing data. Analogously, we also designed CV_{county} and CV_{city}, in which all *in situ* observations within the same geographic unit for all dates were simultaneously used as the testing data. In CV_{county} or CV_{city}, observations from 20% of randomly selected counties or cities were left out of the training data. Interpretation of the CV results depends on different applications of the fused O₃ estimates. For instance, in China, the current monitoring network covers all of the cities; therefore, CV_{city} which assumes no other monitoring for the cities involved in the testing subset, may be less representative for practical purposes. To assess how the data-fusion estimator performs for the counties not covered by the monitoring network, the CV_{county} results should be utilized. In addition, we tested whether the estimates could be utilized in trend analyses, based on the CV results. Given the representativeness of CV_{county}, we analyzed the county trends. We compared the trends derived from testing data to those derived from the corresponding predictions. In this way, we examined how the

final estimator predicted the trend of O₃ for a county without any monitoring sites.

Trend Analyses. We used our product to assess the O₃ exposure in China and analyze its spatiotemporal trends. The exposure at a national or regional scale was characterized by population-weighted statistics (e.g., the mean and percentiles). To quantify the temporal pattern, we calculated the least-squares trends, as per previous studies.³⁵ First, we calculated the anomalies by removing the periodic signals from the time series of O₃ at a specific location (using the R-function, decompose) and then regressed the anomalies with the time index. The regression coefficient and its confidential intervals were used to evaluate the trends in O₃. To compare the trends of O₃ to those of PM_{2.5}, we obtained PM_{2.5} estimates (for 2013–2017) based on a similar data fusion approach.²² The PM_{2.5} estimates have the same spatial and temporal resolutions as the O₃ estimates, so the two datasets can be directly compared. The PM_{2.5} estimates have been used widely in previous studies to evaluate air quality changes and their health impacts during China's clean-air actions.^{5,16}

RESULTS

CV of the O₃ Estimates. Figure 2 presents the CV results for the CMAQ + satellite + monitor estimator at different timescales. Based on the CV_S, the CMAQ + satellite + monitor

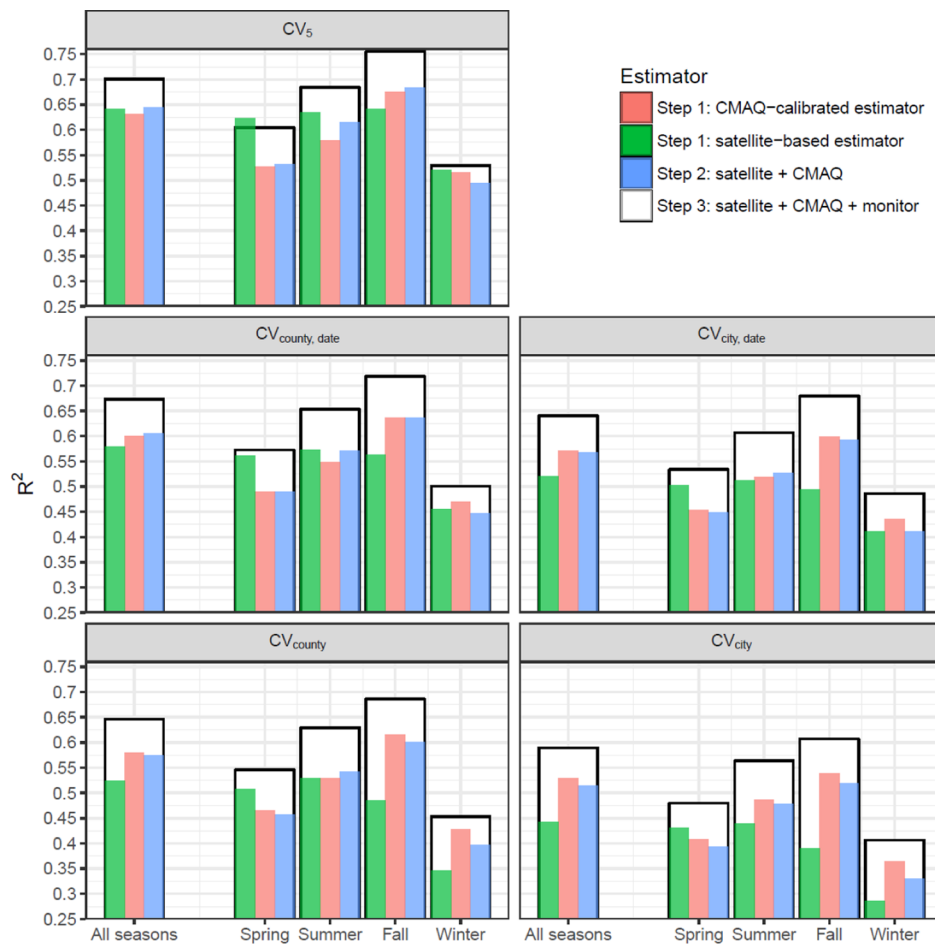


Figure 3. Correlation between observations and model estimates for all data and also by season for different CV approaches.

estimator of MDA8 O₃ is in good agreement with the *in situ* observations. For all-season values, $R^2 = 0.70$, and the RMSE = 26 $\mu\text{g}/\text{m}^3$, which accounts for 29% of the mean value (RPE = 29%). Previous studies^{7,13} have evaluated O₃ exposure based on summer values. Therefore, we also visualized the CV results during the summer months (JJA), which resulted in $R^2 = 0.68$ and RMSE = 28 $\mu\text{g}/\text{m}^3$, both of which are similar to the all-season statistics. These results suggest that our final estimator can well predict the high O₃ values during summer. In epidemiological studies, long-term exposure to O₃ has been evaluated based on average MDA8 O₃ values during the warm season.¹³ Therefore, to examine whether the final estimator is suitable for assessing long-term O₃ exposure, we also summarized the CV₅ results, after aggregating the daily summer values into monthly and annual averages. The CMAQ + satellite + monitor estimator performs better on a monthly (RPE = 18%) or annual scale (RPE = 15%), compared to the daily results (PRE = 26%), because averaging can reduce random errors.

Model performance improves with data-fusion steps (Figure S1). For instance, the CMAQ-calibrated estimator has an $R^2 = 0.59$, which increased to 0.62 for the CMAQ + satellite estimator and further increased to 0.68 for the CMAQ + satellite + monitor estimator. Although the step 1 satellite-based estimator ($R^2 = 0.63$) outperforms the CMAQ-calibrated estimator (step 1) and CMAQ + satellite estimator (step 2), it has lower coverage (44%) than the other estimators (100%) due to the missing values in satellite-derived O₃. An

example of missing data is shown in Figure S2. For the summer values, the key indicators for the health effect of O₃, the satellite-based estimator (step 1), were optimal (as shown by the CV₅ panel in Figure 3), which highlights the essentiality of incorporating the satellite product into data fusion.

Figure 3 presents model performance (assessed by CV R^2 s) by season for different CV approaches. For the CMAQ + satellite + monitor estimator, the seasonal variation in model performance is similar for all CV approaches. The correlation between CMAQ + satellite + monitor estimates and observations is highest in fall (Sep-Oct-Nov), followed by summer (Jun-Jul-Aug), spring (Mar-Apr-May), and winter (Dec-Jan-Feb). The model performance also varied with the CV approach, and comparing them shows that the prediction capacity is sensitive to the coverage of monitoring networks. In general, missing *in situ* observations for larger spatiotemporally clustered units leads to worse model performance. For instance, in the training data for CV_{county}, when there was no monitoring value for a certain county, the *in situ* observations from its neighboring counties contribute to predictions; in contrast, in the training data of CV_{city}, observations from the target county and its neighbors within the same city were absent, which explains the lower CV_{city} R^2 (0.59) than for CV_{county} ($R^2 = 0.65$).

For the step 1 and 2 estimators, model performance varies in a complex way with different CV approaches. Approximately speaking, the satellite-based estimator (step 1) is sensitive to coverage of the *in situ* networks. For instance, compared to the

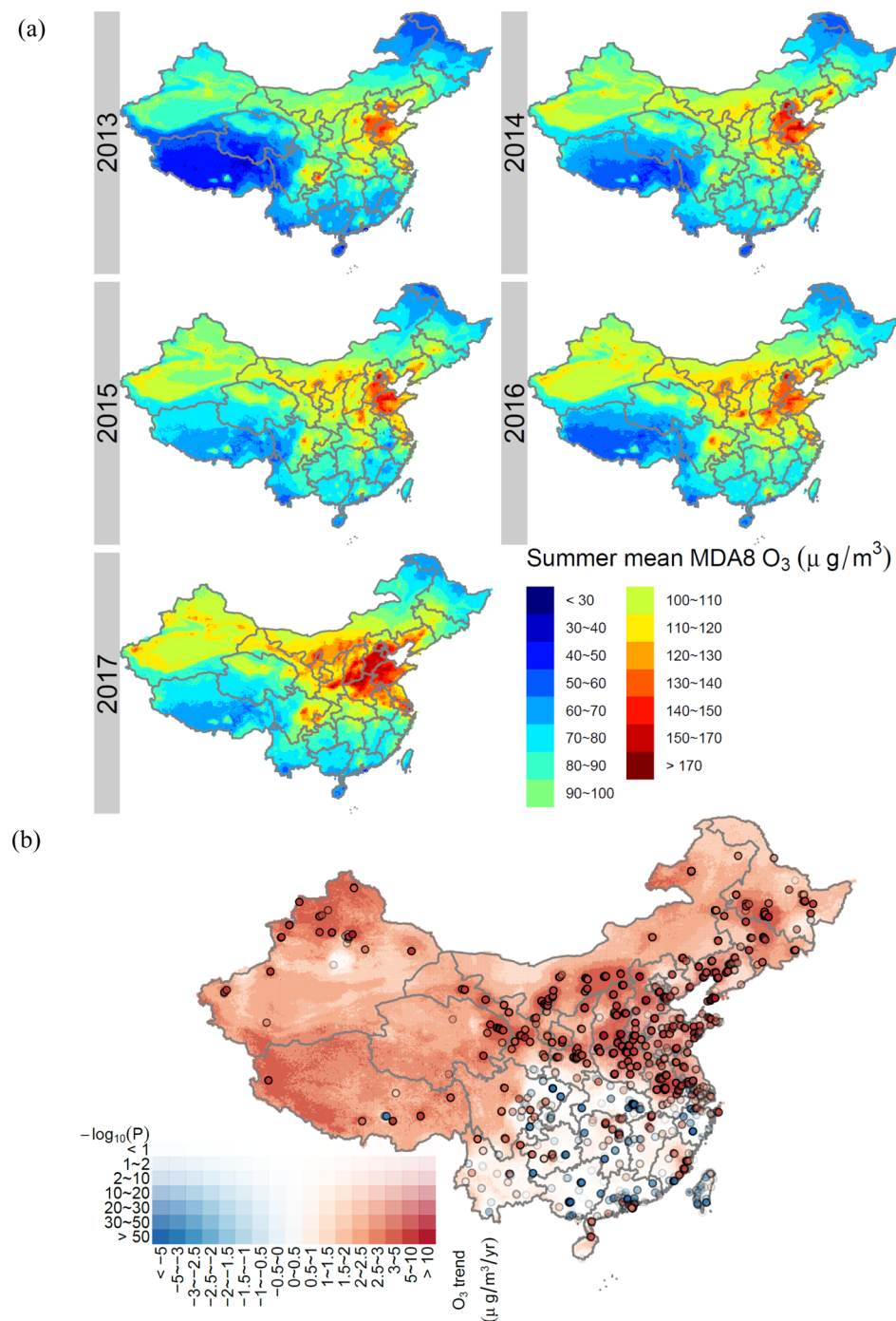


Figure 4. Spatiotemporal variation in the estimated O_3 in China. Panel (a) presents the average of MDA8 O_3 in summer by year, and panel (b) presents the least-squared trends in the estimated O_3 by pixel. Panel (b) also displays the corresponding trends in monitoring observations (dots). In the panel (b), a significant level of trends is evaluated by P values and visualized by transparency.

CV_5 result ($R^2 = 0.64$), the CV_{city} R^2 (0.44) for the estimator is considerably smaller; in contrast, the performance of the CMAQ-calibrated estimator is relatively similar (for CV_5 , $R^2 = 0.63$ and for CV_{city} , $R^2 = 0.53$). One possible explanation is the sample size. The satellite measurements only cover 24% of the *in situ* observations (or 44% of the summer observations), but the CMAQ simulations have 100% coverage. Due to the smaller sample size, the satellite random forest model might rely more on the *in situ* networks, compared to the CMAQ model.

Spatiotemporal Variation in O_3 Exposure in China.

Figure 4 presents the spatiotemporal variation in estimated O_3 in China. The mean summer O_3 increased from $97.0 \mu\text{g}/\text{m}^3$ in 2013 to $113.2 \mu\text{g}/\text{m}^3$ in 2017; the duration of the O_3 -polluted period (defined as $MDA8 O_3 > 100 \mu\text{g}/\text{m}^3$) increased from 110.4 days (37.9 of them occurred during summer) in 2013 to 140.3 days (52.9 in summer) in 2017. A more detailed summary of statistics is given in Table 1, which consistently indicates an increasing trend of O_3 exposure on a nationwide scale. To increase the representativeness for long-term exposure, we analyzed the spatial pattern of O_3 by averaging

Table 1. Population-Weighted Statistics for O₃ Exposure in China by Year and Season

	year	mean ($\mu\text{g}/\text{m}^3$)	percentile ($\mu\text{g}/\text{m}^3$)					days of O ₃ $>x \mu\text{g}/\text{m}^3$	
			2.5%	25%	50%	75%	97.5%	$x = 100$	$x = 160$
annual	2013	86.4	42.6	63.0	84.2	106.6	139.1	110.4	9.3
	2014	83.2	40.8	58.9	79.6	104.0	137.4	98.0	10.5
	2015	83.8	36.7	57.3	79.9	107.2	142.7	106.8	12.7
	2016	87.2	40.5	60.9	83.9	110.1	145.9	116.3	14.2
	2017	94.9	45.2	66.8	90.0	119.0	160.4	140.3	24.7
spring	2013	97.1	60.3	78.5	93.9	112.5	144.2	37.1	2.8
	2014	90.3	55.4	73.5	88.2	104.9	131.8	28.8	2.2
	2015	93.2	56.0	72.6	89.6	109.8	143.0	33.2	3.5
	2016	99.3	61.8	80.2	96.2	115.8	146.0	40.9	3.7
	2017	110.3	68.5	87.3	105.5	129.2	167.7	52.2	8.2
summer	2013	97.0	60.9	79.5	95.2	112.7	138.4	37.9	4.7
	2014	102.3	65.3	83.8	100.4	118.5	145.9	43.0	6.7
	2015	103.0	63.4	83.3	101.1	120.7	148.4	44.7	6.9
	2016	106.0	65.6	85.8	104.0	124.4	151.9	48.7	7.4
	2017	113.2	68.9	92.1	111.3	132.2	164.0	52.9	13.2
fall	2013	82.0	44.0	60.9	80.0	101.4	126.3	25.1	1.3
	2014	80.0	42.4	60.8	77.4	97.9	124.0	22.4	1.6
	2015	80.6	36.1	55.7	77.7	103.2	133.4	25.1	2.3
	2016	81.2	39.5	56.4	74.8	102.8	139.2	22.9	3.1
	2017	85.5	45.6	62.8	79.9	104.8	140.9	25.5	3.2
winter	2013	69.1	39.0	52.4	66.9	84.3	105.1	10.3	0.5
	2014	59.5	36.5	48.5	58.8	69.5	85.2	3.8	0.1
	2015	57.7	32.2	45.3	56.7	69.1	86.4	3.7	0.1
	2016	62.3	35.7	49.5	61.2	74.8	91.0	3.8	0.0
	2017	70.0	38.8	56.7	69.6	83.0	102.0	9.7	0.1

summer values only (Figure 4a). The metropolitan area of Beijing has the highest values, and its surroundings (*i.e.*, the North China Plain, including Beijing, Tianjin, the southern region of Hebei province, the northwest region of Shandong province, and the northern region of Henan province) make up the largest contiguous region of O₃ pollution. Other hotspots are highly clustered in metropolitan areas, including the Yangtze River Delta, Chengdu, Chongqing, Wuhan, and the Pearl River Delta. In addition, possibly because of the fluctuation in the climate, other cities (*e.g.*, Xi'an and Shenyang) can also be identified as pollution hotspots in specific years.

Trends of O₃ Exposure, Compared to PM_{2.5}. First, we examined whether the estimates are representative of the spatiotemporal trends of O₃ in China, based on the results of CV_{county} (Figure S3). We found that the county trends derived from estimates were in good agreement ($R^2 = 0.57$) with those derived from the *in situ* observations. It should be noted that the trends in O₃ might be underestimated because of oversmoothing in the predictions (the slope equals 0.63 for a linear regression of the prediction trends against the observation trends).

Figure 4b presents spatiotemporal trends of O₃ in China. The gridded map of the least-squares trend shows that O₃ concentrations significantly increased in north and southwest China, except for in a few places, such as Beijing. In south China, there is no clear trend. We did not find any contiguous region where O₃ is significantly decreased. The national average O₃ increased by 2.07 $\mu\text{g}/\text{m}^3/\text{year}$ (95% CI: 1.65, 2.48); for the major metropolitan areas, Beijing-Tianjin-Hebei, Yangtze River Delta, and Pearl River Delta, the increase is estimated to be 3.54 $\mu\text{g}/\text{m}^3/\text{year}$ (95% CI: 2.84, 4.24), 1.88

$\mu\text{g}/\text{m}^3/\text{year}$ (95% CI: 1.15, 2.62), and $-0.69 \mu\text{g}/\text{m}^3/\text{year}$ (95% CI: -1.84, 0.46), respectively (Figure S4).

In contrast to the spatiotemporal trend of O₃, PM_{2.5} concentrations have significantly decreased in most areas of China (Figure S5). To compare the trends of O₃ with those of PM_{2.5}, we present their correlations in a gridded map (Figure S6). As expected, PM_{2.5} and O₃ are negatively correlated in the north (latitude $>\sim 29^\circ\text{N}$) but positively correlated in the south (latitude $<\sim 29^\circ\text{N}$); this is consistent with previous findings.³⁶ To explore how these covaried trends in O₃ and PM_{2.5} influenced the air quality in China, we calculated the fraction of population that was exposed to the polluted levels of O₃ ($>100 \mu\text{g}/\text{m}^3$) or PM_{2.5} ($>35 \mu\text{g}/\text{m}^3$), as shown in Figure 5a. During winter, PM_{2.5} was the dominant air pollutant, and more than half of the population was exposed to polluted PM_{2.5}. During summer, the fraction of polluted PM_{2.5} was comparable to the fraction of polluted O₃ before 2015, while the former became lower than the latter in 2016 and 2017. According to the spatial distribution of polluted days (Figure 5b), a shift in the dominant species (from PM_{2.5} to O₃) occurred in coastal and high-altitude regions.

DISCUSSION

The study presents estimations of MDA8 O₃ concentrations across China during 2013–2017, by combining the CTM output, *in situ* observations, and satellite measurements. The estimates are in good agreement with the observed data and can be utilized to characterize O₃ exposure and its spatiotemporal variation in China. Based on the estimates, we quantified the trends in O₃ and compared them with the trends in PM_{2.5}. We found that in north China, O₃ varies in the opposite direction to PM_{2.5} and significantly increased after conducting clean-air actions.

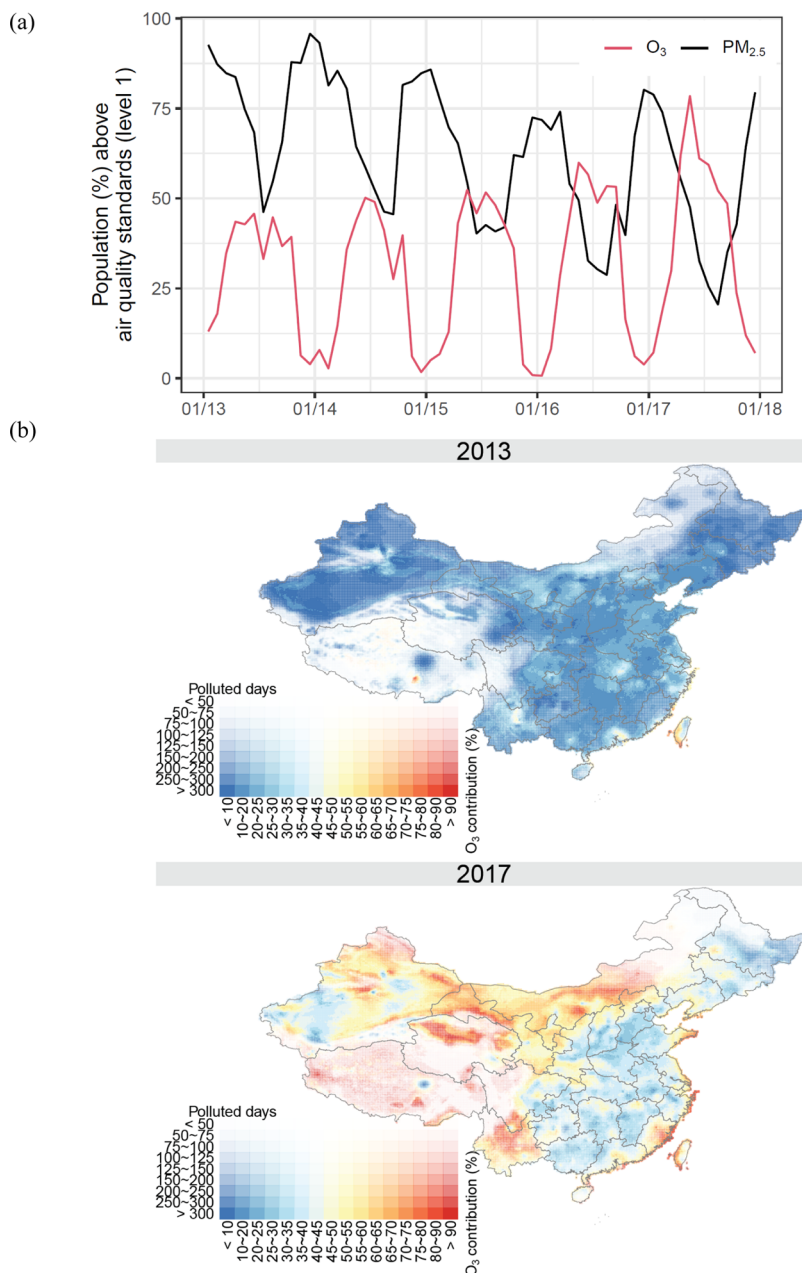


Figure 5. Contributions to the air pollution from O_3 and $PM_{2.5}$. Panel (a): fraction of polluted days (defined as O_3 or $PM_{2.5}$ above China's level I air quality standards) by month; panel (b): contributions to the total number of polluted days from O_3 or $PM_{2.5}$ in 2013 and 2017.

Comparison with Previous Studies. Some studies estimate spatiotemporal variation in O_3 in China, based on land-use regressions, random forests, and statistical interpolation. Zhan *et al.* (2018) claimed the first nationwide statistical modeling study of ambient O_3 for China and estimated the daily MDA8 O_3 in 2015 with RMSE = $26 \mu\text{g}/\text{m}^3$ and RPE = 31%.³⁷ The model incorporated *in situ* observations, meteorological variables, and emission inventories (CTM inputs) into a random forest.³⁷ The accuracy of our model (RMSE = $26 \mu\text{g}/\text{m}^3$, RPE = 29%, as shown in Figure 2) is comparable to this. The 2015 population-weighted mean O_3 exposure was $84 \mu\text{g}/\text{m}^3$, which is also consistent with our findings ($83.8 \mu\text{g}/\text{m}^3$, as shown in Table 1). CTM-based¹⁹ or satellite-based³⁸ estimates of O_3 have also been developed for China, but their model performance was not as good as the results from the random forest model. Similar approaches have

also been applied to derive O_3 estimates for subregions of China, such as Nanjing³⁹ and Hainan.⁴⁰ In addition, data-fusion approaches have been successfully utilized to estimate the O_3 exposure in Los Angeles (*in situ* observations + dispersion model + CTM),⁴¹ Georgia (*in situ* observations + CTM),⁴² and the contiguous United States (*in situ* observations + CTM + satellite O_3).⁴³ All of these studies show that data fusion can efficiently improve model performance of O_3 estimation. Given our unique study period, our data-fusion model is the first state-of-the art database to evaluate continuous spatiotemporal variation in O_3 pollution during China's clean air actions.

In situ observations,^{44,45} CTM simulations,⁴⁶ and satellite measurements,²¹ alone or combined,^{7–9} show the increased trend in ground surface O_3 in China. For instance, Fan *et al.* analyzed the *in situ* observations of the nationwide monitoring

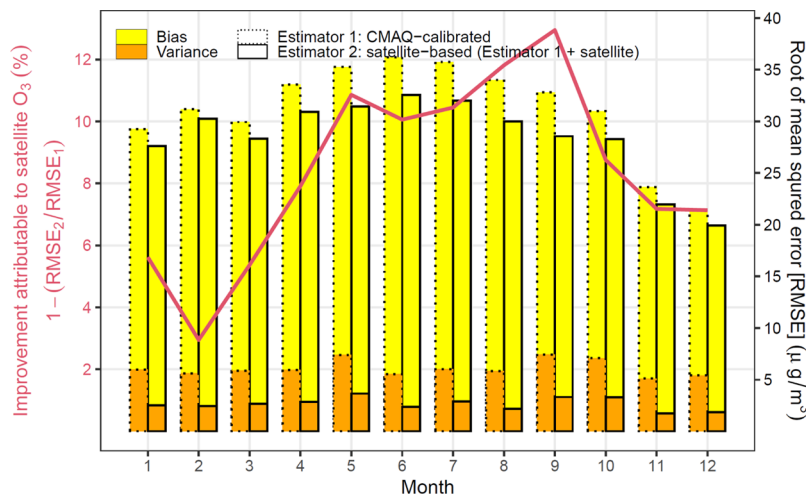


Figure 6. Comparison of modeling errors (measured using the RMSE of the five-fold CV results) of the random forest with satellite-derived O_3 to those without the satellite estimator, by month. The contribution from the satellite-derived O_3 to model performance is quantified by relative reduction in the modeling errors, after incorporating the variable into the random forest.

networks during 2014–2018 and reported that the MDA8 O_3 increased by 4.8% per year.⁴⁴ Based on satellite-derived O_3 , Shen *et al.* found that the increased trend existed over a longer time period.²¹ They found that the mean summer O_3 increased by 3.5 ppb, by comparing the satellite data from 2013–2017 to those from 2005–2009. Based on CTM models, Li *et al.* identified the major drivers of the increased trend in O_3 during 2013–2017 and pointed out that the VOC emission reduction could be a strategy to control PM_{2.5} and O_3 simultaneously.^{7,8} Our study confirms the nationwide growth of O_3 pollution in China but also found that the trends vary spatially, from negative to positive. In the future, our model can be used to support detailed analyses of air quality changes for China.

Role of Satellite O_3 in Data Fusion. A novel aspect of our data-fusion model is the incorporation of the satellite product for ground surface O_3 , which has rarely been included in previous exposure assessment models. To explore how this variable improves model performance, we compared the two estimators in step 1 (Figure S1). The satellite-based estimator is identical to the CMAQ-calibrated model plus the satellite data. We quantified the contribution of satellite-derived O_3 to model improvement as the relative reduction in CV₅ RMSE (Figure 6). We found that the increased accuracy from using satellite data occurred during warm months (May–Sep) and the RMSE could be reduced by at least 10%. This may also explain why our estimator (daily $R^2 = 0.68$ for summer MDA8) outperforms the random forest without satellite O_3 ($R^2 = 0.63$ for summer MDA8).³⁷ In addition, the inclusion of satellite-derived O_3 is also critical to capture the episodes, particularly when the CMAQ model greatly underestimated the pollution levels (Figure S2). Using the annual 95 percentile of MDA8 O_3 as an indicator for an O_3 episode, we found that the satellite-based estimator had lower RMSE ($31 \mu\text{g}/\text{m}^3$) and mean bias ($5 \mu\text{g}/\text{m}^3$) than the CMAQ-calibrated estimator (RMSE = $38 \mu\text{g}/\text{m}^3$ and mean bias = $24 \mu\text{g}/\text{m}^3$), as shown in Figure S7. To further illustrate the roles of different input variables in characterizing an O_3 episode, we compared the estimators with the original CMAQ simulations for a heavily polluted date (29 July 2016) in Figure S2. In this example, when CMAQ failed to predict the high O_3 , calibrating them by the *in situ* observations could partially correct the bias. However, in sparsely monitored regions such as the north of Hebei Province, the correction was

not good enough but was further improved by incorporating the satellite measurements (Figure S2). Because our study is the first to utilize the satellite product (*i.e.*, PROFOZ), its contributions to the prediction of ground surface O_3 should be explored further in future studies.

Implications for Health-Related Studies. The health effects of O_3 exposure in China, particularly long-term, are insufficiently studied,^{11,13,14} and this, therefore, might lead to underestimation of the disease burden attributable to O_3 . Long-term exposure to ambient O_3 has been shown to increase the risk for respiratory diseases¹³ and thus contribute to premature deaths due to air pollutants.¹ Besides the respiratory diseases, epidemiological studies have recently shown that O_3 can increase the mortality risk through other channels, such as cardiovascular diseases and metabolism disorders.^{11,14,15} Therefore, the disease burden of O_3 should be re-evaluated in China by carrying out risk assessment studies. To derive the population-representative exposure-response functions for O_3 , a nationwide epidemiology study is warranted. Either the risk assessment or epidemiological studies will depend on the continuous spatiotemporal estimates of O_3 concentrations. Therefore, this study provides state-of-the-art estimates of O_3 , which can support the health-related studies during 2013–2017.

Study Limitations. This study is subject to the following limitations. First, due to the complicated multiple-step data fusion, the model cannot generate pointwise uncertainty ranges, such as standard errors or confidence intervals, for the O_3 estimates. Therefore, when using the estimates in future health-related studies, potential exposure misclassification may not be completely avoided and the implications should be cautiously explored. Second, the spatial resolution of our estimates is limited due to the current availability of satellite measurements of O_3 . The OMI O_3 profile has a resolution of $13 \times 24 \text{ km}$, which might not be able to capture the fine-scale variation in O_3 . Therefore, when using our product, health-related studies should be at a national or subnational scale and rely on intercity variation rather than intracity variation in O_3 . Third, also due to the satellite data, the temporal resolution of the combined estimator is at a daily scale. However, recent epidemiology studies have shown that the maximum hourly value may also be indicative of some adverse health outcomes,

by capturing O₃ episodes.¹⁴ In future studies, other statistics for O₃ exposure should also be developed using a similar data-fusion approach. Fourth, as shown by different CV approaches, our combined estimator greatly depends on the *in situ* observations, which prevents evaluation of the historical concentrations of O₃ before 2013. A hindcast model of O₃, such as the one for PM_{2.5},³⁵ should be considered for this purpose. Fifth, because many different machine learning models have been applied to estimate air pollutants, our algorithm, which aims to explore the use of data fusion, might be improved by incorporating more advanced techniques, such as neural networks.^{43,47} Optimization of our data-fusion model should be explored in future studies. Finally, although the inputted variables in our data-fusion model captured major drivers underlying the photochemical formation of O₃ (*e.g.*, temperature and NO₂), other key factors were ignored due to computational burden. Incorporation of additional variables such as satellite HCHO,⁴⁸ satellite CO,⁴⁹ or CTM-simulated photolysis rate may improve model performance and should be explored in future.

ASSOCIATED CONTENT

Supporting Information

The Supporting Information is available free of charge at <https://pubs.acs.org/doi/10.1021/acs.est.0c03098>.

Details of CVs and spatiotemporal trends (PDF)

AUTHOR INFORMATION

Corresponding Authors

Qiang Zhang — Ministry of Education Key Laboratory for Earth System Modeling, Department of Earth System Science, Tsinghua University, Beijing 100084, China;
Email: qiangzhang@tsinghua.edu.cn

Tong Zhu — BIC-ESAT and SKL-ESPC, Peking University, Beijing 100871, China; orcid.org/0000-0002-2752-7924; Email: tzhu@pku.edu.cn

Authors

Tao Xue — Institute of Reproductive and Child Health / Ministry of Health Key Laboratory of Reproductive Health and Department of Epidemiology and Biostatistics, School of Public Health, Peking University, Beijing 100191, China; orcid.org/0000-0002-7045-2307

Xixuan Zheng — Ministry of Education Key Laboratory for Earth System Modeling, Department of Earth System Science, Tsinghua University, Beijing 100084, China; Center of Air Quality Simulation and System Analysis, Chinese Academy for Environmental Planning, Beijing 100012, China

Guannan Geng — School of Environment, Tsinghua University, Beijing 100084, China; orcid.org/0000-0002-1605-8448

Qingyang Xiao — Ministry of Education Key Laboratory for Earth System Modeling, Department of Earth System Science, Tsinghua University, Beijing 100084, China

Xia Meng — School of Public Health, Key Lab of Public Health Safety of the Ministry of Education, & NHC Key Lab of Health Technology Assessment, Fudan University, Shanghai 200032, China

Meng Wang — Department of Epidemiology and Environmental Health, School of Public Health and Health Professions, University at Buffalo, Buffalo, New York 14214, United States

Xin Li — Department of Environmental Science and Engineering, Beijing Technology and Business University, Beijing 100048, China; orcid.org/0000-0003-2202-6829

Nana Wu — Ministry of Education Key Laboratory for Earth System Modeling, Department of Earth System Science, Tsinghua University, Beijing 100084, China

Complete contact information is available at:
<https://pubs.acs.org/10.1021/acs.est.0c03098>

Author Contributions

T.Z., Q.Z., and T.X. designed the study; T.X., Y.Z., G.G., X.L., and W.N. prepared the data; T.X., Y.Z., and G.G. analyzed the data; T.X., Y.Z., G.G., Q.X., X.M., and M.W. drafted the manuscript, and all coauthors revised and approved it together.

Funding

This work was supported by Energy Fund (G-1811-28843), National Natural Science Foundation of China (41701591, 81571130100, 41421064, and 41921005), Ministry of Science and Technology of China (2015CB553401), and the Second Tibetan Plateau Scientific Expedition and Research (2019QZKK0607).

Notes

The authors declare no competing financial interest.

REFERENCES

- (1) Lelieveld, J.; Evans, J. S.; Fnais, M.; Giannadaki, D.; Pozzer, A. The contribution of outdoor air pollution sources to premature mortality on a global scale. *Nature* **2015**, *525*, 367–371.
- (2) Anenberg, S. C.; Henze, D. K.; Tinney, V.; Kinney, P. L.; Raich, W.; Fann, N.; Malley, C. S.; Roman, H.; Lamsal, L.; Duncan, B.; Martin, R. V.; van Donkelaar, A.; Brauer, M.; Doherty, R.; Jonson, J. E.; Davila, Y.; Sudo, K.; Kuylenstierna, J. C. I. Estimates of the global burden of ambient PM_{2.5}, ozone, and NO₂ on asthma incidence and emergency room visits. *Environ. Health Perspect.* **2018**, *126*, 107004.
- (3) Gakidou, E.; Afshin, A.; Abajobir, A. A.; Abate, K. H.; Abbafati, C.; Abbas, K. M.; Abd-Allah, F.; Abdulle, A. M.; Abera, S. F.; Aboyans, V. Global, regional, and national comparative risk assessment of 84 behavioural, environmental and occupational, and metabolic risks or clusters of risks, 1990–2016: a systematic analysis for the Global Burden of Disease Study 2016. *Lancet* **2017**, *390*, 1345–1422.
- (4) Zhang, Q.; Zheng, Y.; Tong, D.; Shao, M.; Wang, S.; Zhang, Y.; Xu, X.; Wang, J.; He, H.; Liu, W.; Ding, Y.; Lei, Y.; Li, J.; Wang, Z.; Zhang, X.; Wang, Y.; Cheng, J.; Liu, Y.; Shi, Q.; Yan, L.; Geng, G.; Hong, C.; Li, M.; Liu, F.; Zheng, B.; Cao, J.; Ding, A.; Gao, J.; Fu, Q.; Huo, J.; Liu, B.; Liu, Z.; Yang, F.; He, K.; Hao, J. Drivers of improved PM_{2.5} air quality in China from 2013 to 2017. *Proc. Natl. Acad. Sci.* **2019**, *116*, 24463–24469.
- (5) Xue, T.; Liu, J.; Zhang, Q.; Geng, G.; Zheng, Y.; Tong, D.; Liu, Z.; Guan, D.; Bo, Y.; Zhu, T.; He, K.; Hao, J. Rapid improvement of PM_{2.5} pollution and associated health benefits in China during 2013–2017. *Sci. China Earth Sci.* **2019**, *62*, 1847–1856.
- (6) Huang, J.; Pan, X.; Guo, X.; Li, G. Health impact of China's Air Pollution Prevention and Control Action Plan: an analysis of national air quality monitoring and mortality data. *Lancet Planet. Health* **2018**, *2*, e313–e323.
- (7) Li, K.; Jacob, D. J.; Liao, H.; Shen, L.; Zhang, Q.; Bates, K. H. Anthropogenic drivers of 2013–2017 trends in summer surface ozone in China. *Proc. Natl. Acad. Sci.* **2019**, *116*, 422–427.
- (8) Li, K.; Jacob, D. J.; Liao, H.; Zhu, J.; Shah, V.; Shen, L.; Bates, K. H.; Zhang, Q.; Zhai, S. A two-pollutant strategy for improving ozone and particulate air quality in China. *Nat. Geosci.* **2019**, *12*, 906–910.
- (9) Lu, X.; Hong, J.; Zhang, L.; Cooper, O. R.; Schultz, M. G.; Xu, X.; Wang, T.; Gao, M.; Zhao, Y.; Zhang, Y. Severe surface ozone pollution in China: A global perspective. *Environ. Sci. Technol. Lett.* **2018**, *5*, 487–494.

- (10) Wang, W.-N.; Cheng, T.-H.; Gu, X.-F.; Chen, H.; Guo, H.; Wang, Y.; Bao, F.-W.; Shi, S.-Y.; Xu, B.-R.; Zuo, X. Assessing spatial and temporal patterns of observed ground-level ozone in China. *Sci. Rep.* **2017**, *7*, 3651.
- (11) Turner, M. C.; Jerrett, M.; Pope, C. A., III; Krewski, D.; Gapstur, S. M.; Diver, W. R.; Beckerman, B. S.; Marshall, J. D.; Su, J.; Crouse, D. L.; Burnett, R. T. Long-term ozone exposure and mortality in a large prospective study. *Am. J. Respir. Crit. Care Med.* **2016**, *193*, 1134–1142.
- (12) Lim, C. C.; Hayes, R. B.; Ahn, J.; Shao, Y.; Silverman, D. T.; Jones, R. R.; Garcia, C.; Bell, M. L.; Thurston, G. D. Long-term exposure to ozone and cause-specific mortality risk in the United States. *Am. J. Respir. Crit. Care Med.* **2019**, *200*, 1022–1031.
- (13) Jerrett, M.; Burnett, R. T.; Pope, C. A., III; Ito, K.; Thurston, G.; Krewski, D.; Shi, Y.; Calle, E.; Thun, M. Long-term ozone exposure and mortality. *N. Engl. J. Med.* **2009**, *360*, 1085–1095.
- (14) Kazemiparkouhi, F.; Eum, K.-D.; Wang, B.; Manjourides, J.; Suh, H. H. Long-term ozone exposures and cause-specific mortality in a US Medicare cohort. *J. Expo. Sci. Environ. Epidemiol.* **2019**, *30*, 650–658.
- (15) Yin, P.; Chen, R.; Wang, L.; Meng, X.; Liu, C.; Niu, Y.; Lin, Z.; Liu, Y.; Liu, J.; Qi, J.; You, J.; Zhou, M.; Kan, H. Ambient ozone pollution and daily mortality: a nationwide study in 272 Chinese cities. *Environ. Health Perspect.* **2017**, *125*, 117006.
- (16) Zheng, Y.; Xue, T.; Zhang, Q.; Geng, G.; Tong, D.; Li, X.; He, K. Air quality improvements and health benefits from China's clean air action since 2013. *Environ. Res. Lett.* **2017**, *12*, 114020.
- (17) Xue, T.; Zhu, T.; Zheng, Y.; Liu, J.; Li, X.; Zhang, Q. Change in the number of PM_{2.5}-attributed deaths in China from 2000 to 2010: Comparison between estimations from census-based epidemiology and pre-established exposure-response functions. *Environ. Int.* **2019**, *129*, 430–437.
- (18) Burnett, R. T.; Pope, C. A., III; Ezzati, M.; Olives, C.; Lim, S. S.; Mehta, S.; Shin, H. H.; Singh, G.; Hubbell, B.; Brauer, M.; Anderson, H. R.; Smith, K. R.; Balmes, J. R.; Bruce, N. G.; Kan, H.; Laden, F.; Prüss-Ustün, A.; Turner, M. C.; Gapstur, S. M.; Diver, W. R.; Cohen, A. An integrated risk function for estimating the global burden of disease attributable to ambient fine particulate matter exposure. *Environ. Health Perspect.* **2014**, *122*, 397–403.
- (19) Liu, H.; Liu, S.; Xue, B.; Lv, Z.; Meng, Z.; Yang, X.; Xue, T.; Yu, Q.; He, K. Ground-level ozone pollution and its health impacts in China. *Atmos. Environ.* **2018**, *173*, 223–230.
- (20) Travis, K. R.; Jacob, D. J.; Fisher, J. A.; Kim, P. S.; Marais, E. A.; Zhu, L.; Yu, K.; Miller, C. C.; Yantosca, R. M.; Sulprizio, M. P.; Thompson, A. M.; Wennberg, P. O.; Crounse, J. D.; Clair, J. M.; Cohen, R. C.; Laughner, J. L.; Dibb, J. E.; Hall, S. R.; Ullmann, K.; Wolfe, G. M.; Pollack, I. B.; Peischl, J.; Neuman, J. A.; Zhou, X. Why do models overestimate surface ozone in the southeastern United States? *Atmos. Chem. Phys.* **2016**, *16*, 13561.
- (21) Shen, L.; Jacob, D. J.; Liu, X.; Huang, G.; Li, K.; Liao, H.; Wang, T. An evaluation of the ability of the Ozone Monitoring Instrument (OMI) to observe boundary layer ozone pollution across China: application to 2005–2017 ozone trends. *Atmos. Chem. Phys.* **2019**, *19*, 6551–6560.
- (22) Xue, T.; Zheng, Y.; Geng, G.; Zheng, B.; Jiang, X.; Zhang, Q.; He, K. Fusing observational, satellite remote sensing and air quality model simulated data to estimate spatiotemporal variations of PM_{2.5} exposure in China. *Remote Sens.* **2017**, *9*, 221.
- (23) Sarwar, G.; Luecken, D.; Yarwood, G.; Whitten, G. Z.; Carter, W. P. L. Impact of an updated carbon bond mechanism on predictions from the CMAQ modeling system: Preliminary assessment. *J. Appl. Meteorol. Climatol.* **2008**, *47*, 3–14.
- (24) Cressie, N. *Statistics for Spatial Data*; John Wiley & Sons, 2015.
- (25) Liu, X.; Bhartia, P.; Chance, K.; Spurr, R.; Kurosu, T. Ozone profile retrievals from the Ozone Monitoring Instrument. *Atmos. Chem. Phys.* **2010**, *10*, 2521.
- (26) Huang, G.; Liu, X.; Chance, K.; Yang, K.; Bhartia, P. K.; Cai, Z.; Allaart, M.; Ancellet, G.; Calpini, B.; Coetzee, G. J. R.; Cuevas-Agulló, E.; Cupeiro, M.; De Backer, H.; Dubey, M. K.; Fuelberg, H. E.; Fujiwara, M.; Godin-Beekmann, S.; Hall, T. J.; Johnson, B.; Joseph, E.; Kivi, R.; Kois, B.; Komala, N.; König-Langlo, G.; Laneve, G.; Leblanc, T.; Marchand, M.; Minschwaner, K. R.; Morris, G.; Newchurch, M. J.; Ogino, S.-Y.; Ohkawara, N.; Piters, A. J. M.; Posny, F.; Querel, R.; Scheele, R.; Schmidlin, F. J.; Schnell, R. C.; Schrems, O.; Selkirk, H.; Shiotani, M.; Skrívánková, P.; Stübi, R.; Taha, G.; Tarasick, D. W.; Thompson, A. M.; Thouret, V.; Tully, M. B.; Van Malderen, R.; Vömel, H.; von der Gathen, P.; Witte, J. C.; Yela, M. Validation of 10-year SAO OMI Ozone Profile (PROFOZ) product using observations. *Atmos. Meas. Tech.* **2017**, *10*, 2455–2475.
- (27) Huang, G.; Liu, X.; Chance, K.; Yang, K.; Cai, Z. Validation of 10-year SAO OMI ozone profile (PROFOZ) product using Aura MLS measurements. *Atmos. Meas. Tech.* **2018**, *11*, 17.
- (28) McPeters, R. D.; Labow, G. J.; Logan, J. A. Ozone climatological profiles for satellite retrieval algorithms. *J. Geophys. Res. Atmos.* **2007**, *112*, D05308.
- (29) Breiman, L. Random forests. *Mach. Learn.* **2001**, *45*, 5–32.
- (30) Liaw, A.; Wiener, M. Classification and regression by randomForest. *R. News* **2002**, *2*, 18–22.
- (31) Zou, H.; Hastie, T. Regularization and variable selection via the elastic net. *J. R. Stat. Soc. Series B Stat. Methodol.* **2005**, *67*, 301–320.
- (32) Friedman, J.; Hastie, T.; Tibshirani, R. Regularization paths for generalized linear models via coordinate descent. *J. Stat. Software* **2010**, *33*, 1.
- (33) Cressie, N.; Wikle, C. K. *Statistics for Spatio-Temporal Data*; John Wiley & Sons, 2015.
- (34) Datta, G. S.; Lahiri, P. A unified measure of uncertainty of estimated best linear unbiased predictors in small area estimation problems. *Stat. Sin.* **2000**, *10*, 613–627.
- (35) Xue, T.; Zheng, Y.; Tong, D.; Zheng, B.; Li, X.; Zhu, T.; Zhang, Q. Spatiotemporal continuous estimates of PM_{2.5} concentrations in China, 2000–2016: A machine learning method with inputs from satellites, chemical transport model, and ground observations. *Environ. Int.* **2019**, *123*, 345–357.
- (36) Zhu, J.; Chen, L.; Liao, H.; Dang, R. Correlations between PM and ozone over China and associated underlying reasons. *Atmosphere* **2019**, *10*, 352.
- (37) Zhan, Y.; Luo, Y.; Deng, X.; Grieneisen, M. L.; Zhang, M.; Di, B. Spatiotemporal prediction of daily ambient ozone levels across China using random forest for human exposure assessment. *Environ. Pollut.* **2018**, *233*, 464–473.
- (38) Liang, S.; Li, X.; Teng, Y.; Fu, H.; Chen, L.; Mao, J.; Zhang, H.; Gao, S.; Sun, Y.; Ma, Z.; Azzi, M. Estimation of health and economic benefits based on ozone exposure level with high spatial-temporal resolution by fusing satellite and station observations. *Environ. Pollut.* **2019**, *255*, 113267.
- (39) Huang, L.; Zhang, C.; Bi, J. Development of land use regression models for PM_{2.5}, SO₂, NO₂ and O₃ in Nanjing, China. *Environ. Res.* **2017**, *158*, 542–552.
- (40) Li, R.; Cui, L.; Hongbo, F.; Li, J.; Zhao, Y.; Chen, J. Satellite-based estimation of full-coverage ozone (O₃) concentration and health effect assessment across Hainan Island. *J. Clean. Prod.* **2020**, *244*, 118773.
- (41) Wang, M.; Sampson, P. D.; Hu, J.; Kleeman, M.; Keller, J. P.; Olives, C.; Szapiro, A. A.; Vedal, S.; Kaufman, J. D. Combining land-use regression and chemical transport modeling in a spatiotemporal geostatistical model for ozone and PM_{2.5}. *Environ. Sci. Technol.* **2016**, *50*, 5111–5118.
- (42) Friberg, M. D.; Zhai, X.; Holmes, H. A.; Chang, H. H.; Strickland, M. J.; Sarnat, S. E.; Tolbert, P. E.; Russell, A. G.; Mulholland, J. A. Method for fusing observational data and chemical transport model simulations to estimate spatiotemporally resolved ambient air pollution. *Environ. Sci. Technol.* **2016**, *50*, 3695–3705.
- (43) Di, Q.; Rowland, S.; Koutrakis, P.; Schwartz, J. A hybrid model for spatially and temporally resolved ozone exposures in the continental United States. *J. Air Waste Manage. Assoc.* **2017**, *67*, 39–52.

- (44) Fan, H.; Zhao, C.; Yang, Y. A comprehensive analysis of the spatio-temporal variation of urban air pollution in China during 2014–2018. *Atmos. Environ.* **2020**, *220*, 117066.
- (45) Silver, B.; Reddington, C. L.; Arnold, S. R.; Spracklen, D. V. Substantial changes in air pollution across China during 2015–2017. *Environ. Res. Lett.* **2018**, *13*, 114012.
- (46) Liu, Y.; Wang, T. Worsening urban ozone pollution in China from 2013 to 2017—Part 1: The complex and varying roles of meteorology. *Atmos. Chem. Phys.* **2020**, *20*, 6305–6321.
- (47) Seltzer, K. M.; Shindell, D. T.; Kasibhatla, P.; Malley, C. S. Magnitude, trends, and impacts of ambient long-term ozone exposure in the United States from 2000 to 2015. *Atmos. Chem. Phys.* **2020**, *20*, 1757–1775.
- (48) Jin, X.; Fiore, A.; Boersma, K. F.; Smedt, I. D.; Valin, L. Inferring Changes in Summertime Surface Ozone–NO_x–VOC Chemistry over US Urban Areas from Two Decades of Satellite and Ground-Based Observations. *Environ. Sci. Technol.* **2020**, *54*, 6518–6529.
- (49) Zoogman, P.; Jacob, D. J.; Chance, K.; Worden, H. M.; Edwards, D. P.; Zhang, L. Improved monitoring of surface ozone by joint assimilation of geostationary satellite observations of ozone and CO. *Atmos. Environ.* **2014**, *84*, 254–261.